

Structure-based discovery of selective positive allosteric modulators of antagonists for the M₂ muscarinic acetylcholine receptor

Magdalena Korczynska^{a,1}, Mary J. Clark^{b,1}, Celine Valant^{c,1}, Jun Xu^d, Ee Von Moo^c, Sabine Albold^c, Dahlia R. Weiss^a, Hayarpi Torosyan^a, Weijiao Huang^e, Andrew C. Kruse^f, Brent R. Lyda^b, Lauren T. May^c, Jo-Anne Baltos^c, Patrick M. Sexton^c, Brian K. Kobilka^{d,e}, Arthur Christopoulos^{c,2}, Brian K. Shoichet^{a,2}, and Roger K. Sunahara^{b,2}

^aDepartment of Pharmaceutical Chemistry, University of California, San Francisco, CA 94158; ^bDepartment of Pharmacology, University of California San Diego School of Medicine, La Jolla, CA 92093; ^cDrug Discovery Biology, Monash Institute of Pharmaceutical Sciences, Monash University, Parkville, VIC 3052, Australia; ^dBeijing Advanced Innovation Center for Structural Biology, School of Medicine, Tsinghua University, 100084 Beijing, China; ^eDepartment of Molecular and Cellular Physiology, Stanford University School of Medicine, Stanford, CA 94305; and ^fDepartment of Biological Chemistry and Molecular Pharmacology, Harvard Medical School, Boston, MA 02115

Edited by Robert J. Lefkowitz, Howard Hughes Medical Institute and Duke University Medical Center, Durham, NC, and approved January 5, 2018 (received for review October 14, 2017)

Subtype-selective antagonists for muscarinic acetylcholine receptors (mAChRs) have long been elusive, owing to the highly conserved orthosteric binding site. However, allosteric sites of these receptors are less conserved, motivating the search for allosteric ligands that modulate agonists or antagonists to confer subtype selectivity. Accordingly, a 4.6 million-molecule library was docked against the structure of the prototypical M₂ mAChR, seeking molecules that specifically stabilized antagonist binding. This led us to identify a positive allosteric modulator (PAM) that potentiated the antagonist *N*-methyl scopolamine (NMS). Structure-based optimization led to compound '628, which enhanced binding of NMS, and the drug scopolamine itself, with a cooperativity factor (α) of 5.5 and a K_B of 1.1 μ M, while sparing the endogenous agonist acetylcholine. NMR spectral changes determined for methionine residues reflected changes in the allosteric network. Moreover, '628 slowed the dissociation rate of NMS from the M₂ mAChR by 50-fold, an effect not observed at the other four mAChR subtypes. The specific PAM effect of '628 on NMS antagonism was conserved in functional assays, including agonist stimulation of [³⁵S]GTP γ S binding and ERK 1/2 phosphorylation. Importantly, the selective allostery between '628 and NMS was retained in membranes from adult rat hypothalamus and in neonatal rat cardiomyocytes, supporting the physiological relevance of this PAM/antagonist approach. This study supports the feasibility of discovering PAMs that confer subtype selectivity to antagonists; molecules like '628 can convert an armamentarium of potent but nonselective GPCR antagonist drugs into subtype-selective reagents, thus reducing their off-target effects.

GPCR | subtype selectivity | PAM antagonist | docking | structure-based ligand discovery

G-protein-coupled receptors (GPCRs) are the largest family of cell surface receptors and the target of $\sim 27\%$ of marketed drugs (1). The five subtypes (M_{1–5}) of the muscarinic acetylcholine receptor (mAChR) family exemplify this, modulating physiology relevant to mental health, motion perception, salivation, respiration, and excretion. The mAChRs are the targets of approved and investigational drugs for several debilitating conditions such as psychosis (2), Alzheimer's disease (3), motion sickness (4), asthma (5), and incontinence (6), among others. Ideally, medicines for treating these diseases should be devoid of adverse effects mediated by interactions with one or more subtypes of mAChR that are not involved in the targeted disorder. Unfortunately, all five mAChRs share high amino acid sequence identities in their orthosteric sites, and current drugs that act at one subtype frequently interact with others (7). As a consequence, off-target but "on-family" effects are a major cause of adverse drug reactions among the mAChRs. For instance, mAChR antagonists such as darifenacin and tolterodine

that treat incontinence mediated via the M₃ mAChR often lead to dry mouth due to effects at glandular M₁ and M₃ mAChRs, increase heart rate via the M₂ mAChR, or increase drowsiness (6, 8, 9). Such intrafamily off-target effects for the mAChRs have reduced the usefulness of what are otherwise highly effective medicines.

To overcome intrafamily promiscuity of mAChR orthosteric drugs, investigators have begun to target the allosteric sites of these receptors (10, 11). The best-established of these sites, first identified by functional pharmacology (12–16), have recently been structurally characterized by crystallography (17) and are now known to atomic resolution for most mAChR subtypes (M₁–M₄) (17–19). This classical muscarinic allosteric pocket (17) is located just above the orthosteric hormone binding site and is partially formed by extracellular loops, which show greater sequence variation among the mAChR subtypes than is observed for the orthosteric sites, and thus have become the focus for the discovery of subtype-selective allosteric ligands. Positive allosteric modulators (PAMs) could

Significance

The orthosteric binding sites of the five muscarinic acetylcholine receptor (mAChR) subtypes are highly conserved, making the development of selective antagonists challenging. The allosteric sites of these receptors are more variable, allowing one to imagine allosteric modulators that confer subtype selectivity, which would reduce the major off-target effects of muscarinic antagonists. Accordingly, a large library docking campaign was prosecuted seeking unique positive allosteric modulators (PAMs) for antagonists, ultimately revealing a PAM that substantially potentiates antagonist binding leading to subtype selectivity at the M₂ mAChR. This study supports the feasibility of discovering PAMs that can convert an armamentarium of potent but nonselective G-protein-coupled receptor (GPCR) antagonist drugs into subtype-selective reagents.

Author contributions: M.K., M.J.C., and C.V. designed research; M.K., M.J.C., C.V., J.X., E.V.M., S.A., D.R.W., H.T., W.H., A.C.K., B.R.L., L.T.M., and J.-A.B. performed research; B.K.K., A.C., B.K.S., and R.K.S. contributed new reagents/analytic tools; M.K., M.J.C., C.V., J.X., P.M.S., B.K.K., A.C., B.K.S., and R.K.S. analyzed data; and M.K., M.J.C., C.V., J.X., B.K.K., A.C., B.K.S., and R.K.S. wrote the paper.

The authors declare no conflict of interest.

This article is a PNAS Direct Submission.

This open access article is distributed under [Creative Commons Attribution-NonCommercial-NoDerivatives License 4.0 \(CC BY-NC-ND\)](https://creativecommons.org/licenses/by-nc-nd/4.0/).

¹M.K., M.J.C., and C.V. contributed equally to this work.

²To whom correspondence may be addressed. Email: arthur.christopoulos@monash.edu, bshoichet@gmail.com, or rsunahara@ucsd.edu.

This article contains supporting information online at www.pnas.org/lookup/suppl/doi:10.1073/pnas.1718037115/-DCSupplemental.

Published online February 16, 2018.

be specific for one subtype over the other four family members and can convert nonselective but otherwise potent orthosteric agonists and antagonists into selective ligands for a particular receptor subtype (13, 20–22).

Here, we investigated the ability of a structure-based approach to discover allosteric molecules that are cooperative with the binding and activity of M_2 mAChR antagonists. Antagonists, such as scopolamine and atropine, have long been investigated for the treatment of diseases like motion sickness, depression, and blocking cholinergic bradycardia (4, 23–26), but have been limited by intrafamily off-target adverse reactions. By screening a library of 4.6 million compounds for complementarity to the inactive state of the M_2 mAChR, we sought such cooperative modulators for M_2 antagonists. Emerging from this screen was a unique family of triazolo-quinazolines unrelated to previously investigated chemotypes for this target. The ability of these unique antagonist PAMs to confer target selectivity, probe specificity, and activity in native tissues was investigated.

Results

Structure-Based Docking at the M_2 mAChR. Seeking selective PAMs of mAChR antagonists, we docked the 4.6 million-molecule lead-like (27) subset of the ZINC database (28, 29) against the allosteric site observed in the antagonist-bound inactive structure of the M_2 /QNB (19) complex (PDB ID code 3UON). This site lies largely above the plane of the membrane, and three tyrosine residues, Tyr104^{3,33}, Tyr403^{6,51}, and Tyr426^{7,39} (superscripts indicate Ballesteros–Weinstein numbering), separate it from the orthosteric site (Fig. 1*A* and *SI Appendix, Fig. S1 A and B*). Unlike the orthosteric site, which only differs from the orthologous site of the M_3 mAChR by a single residue [Leu226^{ECL2(M3)} → Phe181^{ECL2(M2)}], substitutions in the vestibule are more common, where two receptors can differ by up to 11 substitutions among the 24 residues that define the site (18, 19, 30, 31) (*SI Appendix, Fig. S1 C, D, and G and Table S1*). Each ZINC molecule was docked in multiple orientations and conformations to the vestibule; overall, about 10^{12} molecule–receptor complexes were sampled. Each was scored using the physics-based scoring function in DOCK3.6 (32, 33) that calculates van der Waals (34) and electrostatic complementarity (35–37); the latter is corrected for context-dependent ligand desolvation (30, 32). The best-scoring configuration of each molecule in the library was retained, and the library was ranked from best to worst scoring. The docked molecules tiled the vestibular M_2 mAChR allosteric site densely (Fig. 1*A*).

The top 2,000 docking-ranked compounds (top 0.04% of the docked library) were visually inspected and prioritized, based on features not captured by the DOCK3.6 scoring function (38), such as chemical diversity in addition to their docking rank. Ultimately, 13 compounds were picked as potential ligands for the extracellular vestibule of the M_2 mAChR (*SI Appendix, Table S2*), most making unique combinations of interactions with the site (Fig. 1*B–D*). What turned out to be the three active molecules exemplify the different docked geometries and interactions. ZINC00088573 stacks with Trp422^{7,35}, a residue that changes rotamers between the agonist versus the PAM/agonists (LY2119620) or antagonist-bound receptor structures (17), and on the other side of the vestibule the '573 compound stacks with Tyr177 from extracellular loop 2. This creates a four-layered aromatic stacking system that would wedge the vestibule into an open and inactive conformation (Fig. 1*C*). Meanwhile, ZINC00350029 engages the same Tyr177^{ECL2} (Fig. 1*B*) but does not engage Trp422^{7,35}. Additionally, '029 made unique interactions with Asn410^{6,58}. Finally, ZINC05277589 docks directly above the three-conserved tyrosines that form a “septum” between the orthosteric and allosteric sites (Fig. 1*A*). The triazolo-quinazolinone scaffold of '589 orients to π -stack with Tyr403^{6,51} or Tyr426^{7,39} (Fig. 1*D*), while hydrogen-bonding with the backbone of Ile178, potentially stabilizing the position of extracellular loop 2. In addition, the ester moiety of '589 forms a hydrogen bond with the side chain of Asn419^{ECL3}. As shown below, '589 proved to be a PAM for antagonists and was the focus for subsequent structure–activity relationship (SAR) studies.

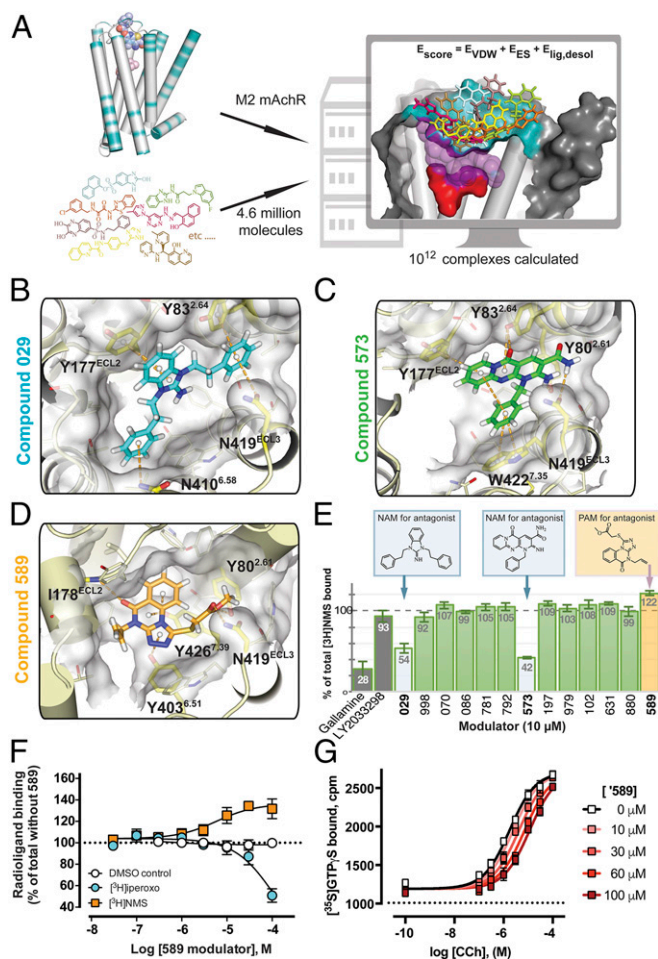


Fig. 1. A structure-based docking screen for allosteric modulators of human M_2 mAChR antagonists. (*A*) The initial docking approach. Seven representative high-ranking docking hits illustrate tiling of the allosteric site (cyan). The orthosteric site is colored red, while residues separating the two sites are presented as purple spheres. Docking poses of (*B*) the NAM '029, (*C*) the NAM '573, (*D*) and the PAM '589 for NMS. Modeled hydrogen bonds and hydrophobic interactions are indicated as dashed lines. (*E*) The effects on [3 H]NMS binding of 10 μ M of the 13 initial docking hits. The structures of three active modulators are shown (docking ranks in *SI Appendix, Table S2*). (*F*) Equilibrium binding between 0.2 nM [3 H]NMS (antagonist) or 0.05 nM [3 H]IXO (agonist). Compound '589 displayed a PAM effect with the antagonist radioligand, but a NAM effect with the agonist radioligand. (*G*) In a CCh-mediated [35 S]GTP γ S binding assay, increasing concentrations of '589 promoted a concentration-dependent, but saturable, reduction in agonist potency, consistent with a NAM effect on the agonist.

Receptor Binding of the Initial Docking Hits. The 13 docking hits were purchased for initial experimental testing. Using membranes of CHO cells stably expressing the human M_2 mAChR, we assessed the effect of 10 μ M concentrations of two well-characterized allosteric modulators, the strong negative allosteric modulator (NAM) of both agonists and antagonists, gallamine, and the weak NAM of antagonists, LY2033298, on the specific binding of 0.2 nM [3 H]*N*-methyl-scopolamine ([3 H]NMS), comparing their effects to that of the 13 docking hits (Fig. 1*E*). Consistent with its known NAM activity, gallamine substantially reduced the specific binding of [3 H]NMS, whereas LY2033298 had a small NAM effect on the radioligand. Of the 13 docking hits, 10 did not alter the specific binding of [3 H]NMS and were not further considered. Conversely, three of them, '029, '573, and '589 modulated [3 H]NMS binding (Fig. 1*B–E*). Both '029 and '573 reduced [3 H]NMS binding, suggesting that these were [3 H]NMS NAMs.

More interesting was the activity of **'589**, which increased the binding of the radioligand, consistent with its activity as a PAM of the labeled antagonist.

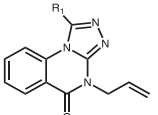
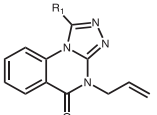
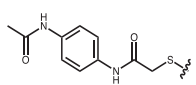
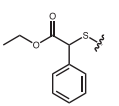
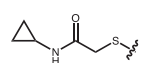
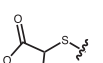
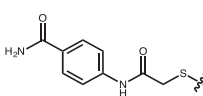
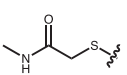
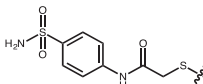
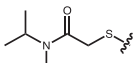
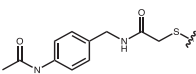
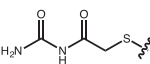
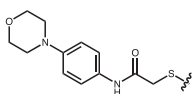
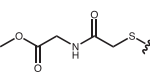
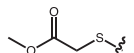
To quantify the effects of **'589** at the M_2 mAChR, we performed equilibrium binding assays with increasing concentrations (0.3–100 μM) of **'589** against two orthosteric radioligands that stabilize distinct receptor conformations; 0.2 nM [^3H]NMS, an antagonist/inverse agonist favoring the inactive state, and 0.05 nM [^3H]iperoxo ([^3H]IXO), an agonist stabilizing the active state (Fig. 1*F*). Consistent with the single concentration screen, **'589** increased antagonist binding by ~20%. Using an allosteric ternary complex model (ATCM), we quantified the affinity (pK_B) of **'589** for the allosteric site on the free receptor and its cooperativity (α) with [^3H]NMS: $\text{pK}_B = 5.35 \pm 0.27$ and $\text{Log}\alpha_{\text{NMS}} = 0.20 \pm 0.03$ ($\alpha_{\text{NMS}} = 1.6$). Strikingly, when switching the orthosteric probe from antagonist to agonist, **'589** reduced [^3H]IXO binding, indicating NAM activity (~50% decrease in binding at the highest concentration tested; Fig. 1*F*). To investigate this agonist NAM activity of **'589** on cellular function, we examined its effects on the promotion of [^{35}S]GTP γS binding to activated G proteins by the agonist carbachol (CCh); this is a prototypical effect mediated by $G_{i/o}$ -coupled receptors such as the M_2 mAChR. Compound **'589** caused a saturable inhibition in CCh's promotion of [^{35}S]GTP γS binding, a hallmark of a NAM with limited negative cooperativity, that is, $\text{Log}\alpha = 0.92 \pm 0.07$ (Fig. 1*G*). To ensure the effect observed was the direct consequence of a drug–receptor interaction, **'589** was tested for colloidal aggregation (38, 39). Whereas particles were seen at 100 μM **'589**, these did not inhibit a classic counterscreening enzyme AmpC β -lactamase, nor was scattering sensitive to detergent, suggesting that the compound was not an aggregator at relevant concentrations.

Structure-Guided Optimization. Using the modeled pose of **'589**, we sought to optimize its affinity by substitutions to the triazolo-quinazolinone scaffold, focusing on groups that could potentially interact with the rim of the allosteric site near Asn419^{ECL3}. This region has been implicated by both mutagenesis (40) and by molecular dynamics simulations (17, 41) as important for allosteric modulator binding. Compounds with three different substitutions were picked: (**R1**) compounds that interacted with the rim of the allosteric site near Asn419^{ECL3}, (**R2**) compounds that test the docking pose of **'589** by clashing with Tyr83^{2,64}, and (**R3**) variations of the hydrophobic group near the Phe181^{ECL2}. Sixteen triazolo-quinazolinone analogs that docked well or, in the case of the **R2** substitutions, docked informatively, were purchased and tested (Table 1 and *SI Appendix, Table S3*); because this was an “analog-by-catalog” exercise, we were not always able to test compounds that measured the effect of one side chain in isolation, as might ordinarily be done in a SAR campaign.

Broadly consistent with these expectations, compounds with larger **R1** groups often increased the potency of the PAMs (Table 1). For instance, ZINC12427**628** had one of the largest **R1** substitutions and displayed the highest affinity ($\text{pK}_B = 5.85 \pm 0.31$) while retaining robust positive cooperativity with the antagonist, that is, $\text{Log}\alpha_{\text{NMS}} = 0.73 \pm 0.16$ ($\alpha_{\text{NMS}} = 5.4$) (Fig. 2*A* and *B* and Table 1). Conversely, compounds that eliminate the ester **R1**-moiety of **'589**, such as ZINC6367**722**, lost most binding cooperativity (*SI Appendix, Table S3*). Switching from an ester to an amide had little effect on total antagonist binding, as observed with the PAM, **'621** (Table 1).

The pose of **'628** changed slightly versus **'589**, partly reflecting our use of the smaller vestibule present in the 4MQT structure that was used for docking at this stage (Fig. 2*C* and *D*). In the docked pose, the carbonyl oxygen of the **R1** moiety appears to bridge Tyr80^{2,61} and Thr423^{7,36}, while the amide nitrogen hydrogen bonds with

Table 1. Allosteric effects of triazolo-quinazolinone analogs of [^3H]NMS-specific binding at the M_2 mAChR

ZINC ID		% [^3H]NMS binding	EC_{50} , μM	pK_B	$\text{Log}\alpha_{\text{NMS}}$ (α_{NMS})	ZINC ID		% [^3H]NMS binding	EC_{50} , μM	pK_B	$\text{Log}\alpha_{\text{NMS}}$ (α_{NMS})
12427 628		163 \pm 11	1.1 \pm 0.4	5.85 \pm 0.31	0.73 \pm 0.16 (5.4)	09635 472		133 \pm 5	11 \pm 3	ND	ND
03590 563		138 \pm 4	2.0 \pm 0.7	4.76 \pm 0.09	0.59 \pm 0.15 (3.8)	03444 509		139 \pm 11	26 \pm 10	ND	ND
02653 768		146 \pm 1	4.8 \pm 0.8	5.03 \pm 0.18	0.23 \pm 0.02 (1.7)	03295 621		125 \pm 6	>50	ND	ND
03245 507		141 \pm 3	7.1 \pm 1.5	5.19 \pm 0.15	0.21 \pm 0.02 (1.6)	03597 405		111 \pm 4	>50	ND	ND
25339 904		146 \pm 5	25.0 \pm 3.7	4.97 \pm 0.14	0.23 \pm 0.03 (1.7)	03572 779		105 \pm 6	ND	ND	ND
03320 344		118 \pm 2	6.7 \pm 0.2	ND	ND	03297 234		107 \pm 3	ND	ND	ND
05277 589		122 \pm 3	21 \pm 7	5.35 \pm 0.27	0.20 \pm 0.03 (1.6)						

Expansion of the scaffold toward Asn419^{6,42} in the allosteric pocket led to the discovery of several unique PAMs on [^3H]NMS binding. Particularly, **'628**, **'563**, **'768**, **'507**, and **'904**, with 50–100% increase in receptors bound by 0.2 nM [^3H]NMS and affinity estimate in the micromolar range. Two-hour radioligand incubation; ND, inactive up to 10 μM . Values represent the mean \pm SEM from at least three experiments performed in duplicate. Bold highlight of ZINC ID indicates shorthand used to refer to compounds. The **'589** row is in bold as it was the initial docking hit.

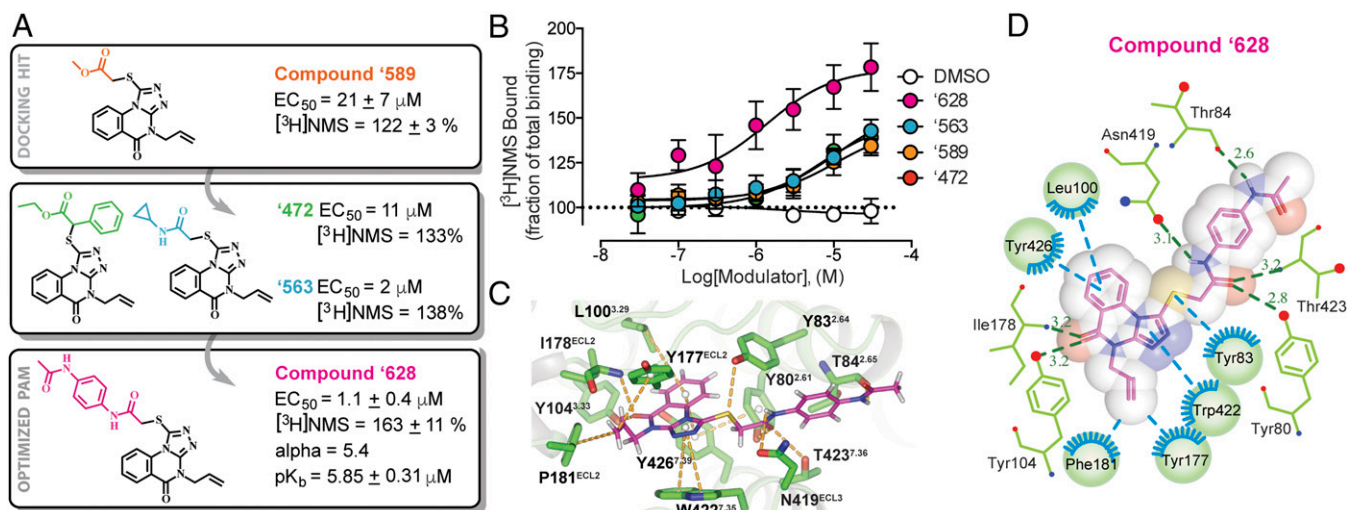


Fig. 2. Structure-guided optimization toward the M_2 mAChR antagonist PAM '628. (A) Changes at the R1 position (Table 1) were most effective at improving activity; best ester and amide-linked PAMs shown. (B) '628 enhances the binding of the antagonist, [3 H]NMS, in M_2 -CHO membranes with an EC_{50} of $1.1 \pm 0.4 \mu\text{M}$. (C) Three-dimensional representation of docking pose of '628. Superscripts indicate Ballesteros-Weinstein numbering. (D) Ligplot representation of the allosteric vestibule with the PAM '628, indicating interactions based on docking pose; hydrogen bonds (green dash) and hydrophobic interactions are indicated (cyan dash).

Asn419^{ECL3}/Glu175^{ECL2}. The bulkier phenyl ring of '628 is modeled to be perpendicular to Tyr83^{2.64}, and the terminal amide substituent, hydrogen bonds with the backbone oxygen of Thr84^{2.65} that caps the TM2 helix. In this optimized docking pose, the five-membered ring of the triazolo-quinazolinone scaffold stacks with Trp422^{7.36}, while the cyclohexane ring is sandwiched between Leu100^{3.29} and Tyr226^{7.39}. Consistent with the steric constraints of the modeled pose, bulky substitutions on the cyclohexane ring at the R2 position result in loss of activity, as with compounds '570 and '567 (SI Appendix, Table S3). Similarly, diminished activity is observed for hydrophobic substitutions that are larger than the original hit at the R3 position, as with compound '094, perhaps caused by steric clashes with the hydrophobic pocket formed by Phe181^{ECL2} and Tyr177^{ECL2}, which in the docking pose of '628 make interaction with the alkene moiety at R3 (Fig. 2 C and D). Mass spectrometry analysis was performed on the purchased '628 compound, indicating that it was pure (SI Appendix, Fig. S2), and subsequent analysis was carried out with this compound.

The Effect on Orthosteric Inverse-Agonist Kinetics and Function of '628. A hallmark of allosteric affinity modulators is their ability to change the association or dissociation rates of orthosteric ligands (42). Since '628 increased the affinity of [3 H]NMS for the M_2 mAChR in equilibrium binding assays, we expected it to alter the dissociation rate of the orthosteric ligands that it modulates. We thus determined the rate of [3 H]NMS dissociation, using isotopic dilution with atropine, in the absence or presence of increasing

concentrations of '628. As the concentration of '628 was increased, the k_{off} of [3 H]NMS from the M_2 mAChR decreased very substantially (~ 50 -fold), so that by $10 \mu\text{M}$ '628 the $t_{1/2}$ was increased to 415 min, compared with 8.2 min without the PAM (Fig. 3A and Table 2). Similarly, in saturation binding assays with [3 H]NMS, the affinity (pK_D) of the antagonist increased with increasing concentrations of modulator, allowing for the determination of a cooperativity factor of $\text{Log}\alpha_{\text{NMS}} = 0.73 \pm 0.06$ (Fig. 3B and Table 2). In contrast, no substantial effect was observed on the affinity of the agonist, [3 H]IXO in analogous saturation binding experiments (Fig. 3C), which was observed for the parent compound '589. This identifies '628 as a neutral allosteric ligand (NAL) of IXO, in contrast to its strong PAM activity against the antagonist NMS.

To assess the allosteric effects of '628 on M_2 mAChR receptor function, we investigated two distinct signaling pathways: [35 S]GTP γ S binding as a direct measure of proximal receptor activation, and ERK1/2 phosphorylation as a measure of downstream and convergent activation. Consistent with the observations from the [3 H]IXO saturation experiments (Fig. 3C), '628 had no appreciable effect on responses to the endogenous agonist, ACh (Fig. 4A and B), or to the high efficacy agonist, IXO (SI Appendix, Fig. S3A and B), confirming its status as a NAL of both agonist function and of agonist binding. This afforded us a rare opportunity to probe allosteric effects on antagonist function without the confounds from agonist modulation. Accordingly, NMS was titrated against a fixed (EC_{80}) concentration of the agonist IXO in the absence or presence of increasing concentrations of '628, and effects on [35 S]GTP γ S

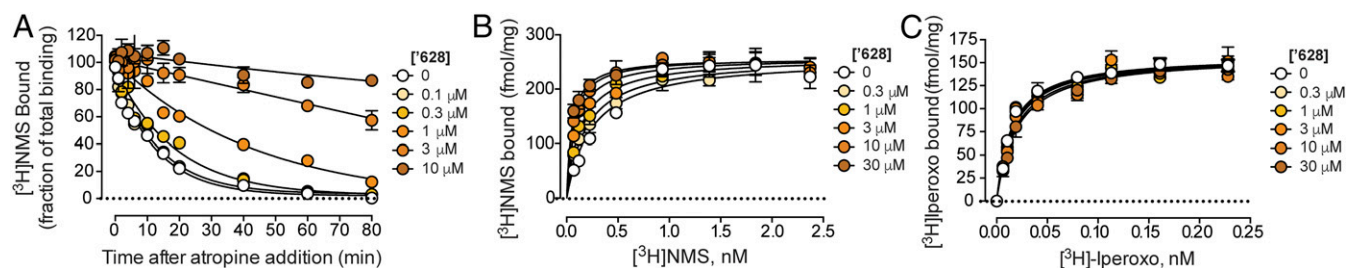


Fig. 3. Characterization of allosteric activity of '628 at M_2 mAChR. (A) Dissociation of 0.2 nM [3 H]NMS was initiated following 1-h incubation by adding $10 \mu\text{M}$ atropine with varying concentrations of '628 or DMSO. The half-life was determined by fitting with a one-phase exponential decay analysis using GraphPad Prism. Saturation binding of (B) [3 H]NMS or (C) [3 H]IXO with varying concentrations of '628 incubated for 2 h at room temperature with membranes from CHO cells stably expressing M_2 mAChR. The binding curves were fit by the allosteric modulator shift analysis using GraphPad Prism.

Table 2. [³H]NMS K_d and dissociation half-life with addition of the allosteric ligand '628 at the five mAChR subtypes

Human mAChR	K_d of [³ H]NMS 2-h incubation		[³ H]NMS dissociation half-life, min		
	Control	+10 μ M '628	Control	+10 μ M '628	Fold increase
M ₁	0.042 \pm 0.010	0.027 \pm 0.003	36 \pm 4	56 \pm 8	1.6
M ₂	0.25 \pm 0.02	0.084 \pm 0.020*	8.2 \pm 0.2	415 \pm 123**	51
M ₃	0.040 \pm 0.009	0.038 \pm 0.009	147 \pm 22	239 \pm 70	1.6
M ₄	0.026 \pm 0.003	0.018 \pm 0.005	68 \pm 3	250 \pm 110	3.7
M ₅	0.089 \pm 0.004	0.11 \pm 0.01	195 \pm 30	157 \pm 14	0.8

* $P < 0.01$, Student's t test; ** $P < 0.0001$, Student's t test.

binding (Fig. 4C, *Left*) and ERK1/2 phosphorylation (Fig. 4D, *Left*) were measured. The neutral cooperativity between '628 and IXO meant that any shift in the antagonist (NMS) inhibition curve solely reflected the functional PAM effect of the modulator on NMS. The resulting antagonist potency estimates (pA_2 values) are shown in Table 3; absolute differences between the two pathways most likely reflect differences in the assay conditions. Irrespective, and most importantly, a plot of each NMS pA_2 estimate as a function of '628 concentration (Fig. 4C and D, *Right*) fitted to the ATCM allowed for the determination of the functional cooperativity between NMS and '628, which was essentially identical between the two pathways: [³⁵S]GTP γ S binding, $\text{Log}\alpha_{\text{NMS}} = 0.73 \pm 0.19$ ($\alpha_{\text{NMS}} = 5.4$); ERK1/2 phosphorylation, $\text{Log}\alpha_{\text{NMS}} = 0.67 \pm 0.20$ ($\alpha_{\text{NMS}} = 4.8$).

Probe Dependence of '628. A common observation with many GPCR allosteric modulators is their "probe dependence," where the magnitude and even direction of the allosteric effect can change dramatically for the same modulator/GPCR pair depending on the orthosteric ligand (43). To determine the differential modulation effects on different orthosteric ligands, that is, the "probe specificity" of '628, we determined its effects on a panel of 17 different orthosteric ligands, including 11 structurally distinct mAChR antagonists, and 6 mAChR agonists of varying degrees of efficacy. All 17 orthosteric ligands were initially assessed in [³H]NMS radioligand titration assays, with increasing concentrations of '628 tested against an EC₈₀ concentration of the orthosteric ligand in the presence of [³H]NMS (Fig. 5A and *SI Appendix*, Fig. S4 and Table S4).

From these probe dependence experiments, three observations seem noteworthy. First, in addition to NMS, '628 was a PAM of two other antagonists, atropine and *N*-desmethyloclozapine (NDMC). The effect on atropine is perhaps unsurprising as it closely resembles NMS. Conversely, several profound functional effects from small chemical changes in the orthosteric probe molecules were unanticipated: thus, '628 is a NAM for clozapine itself, and for tiotropium or ipratropium, for which '628 has negligible binding effects, notwithstanding its strong effects on the related NMS and atropine (Fig. 5A). A second important point is that '628 retained its NAL, or at least nonaffecting, properties for agonists irrespective of the ligand [we infer that '628 is a NAL for agonist as its precursor, '589, inhibited agonist radioligand binding affinity as a NAM (Fig. 1F), although we cannot fully discount the possibility that '628 simply does not bind to receptors in the activated state for most agonists]. Third, '628 was a NAL for most of the other antagonists tested, such as 4-DAMP, QNB, pirenzepine, tiotropium, glycopyrrolate, and ipratropium, most of which are structurally distinct. Intriguingly, '628 had profound NAM activity against himbacine or clozapine. Indeed, the negative cooperativity with himbacine was so pronounced that the interaction was indistinguishable from competition (SI Appendix, Table S4). This observation may be reconciled with himbacine's ability to bind to both the allosteric and orthosteric sites (44). For three of the antagonists—atropine, for which '628 acted as a PAM, and himbacine or clozapine, for which '628 acted as a strong NAM—probe dependence was further tested in functional titration assays, again

using [³⁵S]GTP γ S binding and ERK1/2 phosphorylation (Fig. 5B and C and *SI Appendix*, Fig. S5). Here, the type and magnitude of the functional cooperativity for the three antagonists reflect the observations made in the initial characterizations of the probes in the [³H]NMS binding assay. Fig. 5D summarizes the 17 ligands investigated, their structures, and the type of modulatory effect displayed by '628.

NMR Spectra Support '628s Probe-Dependent Allosteric Function.

Solution NMR spectroscopy, using methionine residues as conformational probes, is used to identify structural changes in the M₂ mAChR that may be used to understand the probe dependence via differential ligand coupling (Fig. 6A). For example, the NMR spectra reveal that tiotropium (Fig. 6B) and NMS (Fig. 6C) stabilize distinct conformations, in agreement with their different functional responses to '628. The incubation of '628 together with NMS caused chemical shifts in spectra for four M₂ mAChR methionine residues: Met77^{2,58}, Met112^{3,41}, Met202^{5,54}, and Met406^{6,54} (Fig. 6D and E). Two of these methionines,

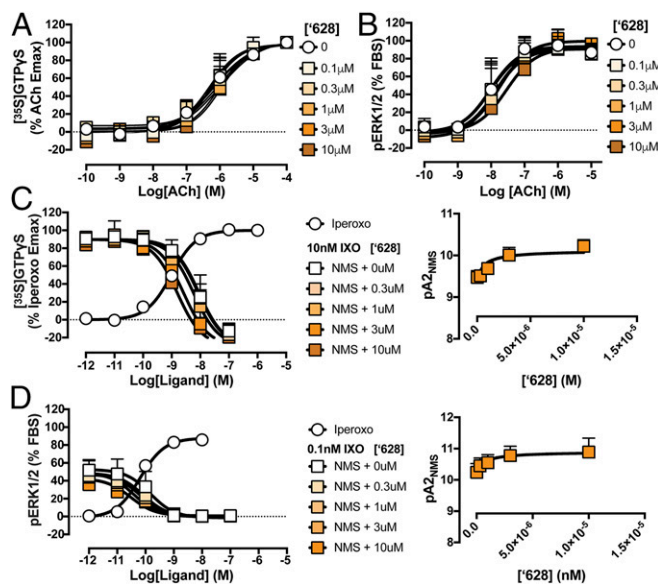


Fig. 4. Functional effects of '628 on agonists and NMS at the M₂ mAChR. Compound '628 was a NAL of the endogenous agonist, ACh, in both (A) [³⁵S]GTP γ S binding and (B) ERK1/2 phosphorylation assays. (C, *Left*) Increasing concentrations of '628 potentiate the ability of NMS to inhibit the function of an EC₈₀ concentration of IXO in a [³⁵S]GTP γ S binding assay; (C, *Right*) increase in NMS potency (pA_2) as a function of modulator concentration. (D, *Left*) Increasing concentrations of '628 potentiate the ability of NMS to inhibit the function of an EC₈₀ concentration of IXO in a ERK1/2 phosphorylation assay; (D, *Right*) increase in NMS potency (pA_2) as a function of modulator concentration. For C and D, *Right*, curves through the points represent the best fit of an ATCM to the data.

Table 3. Affinity estimates (pA_2 values) of NMS in functional assays in absence or presence of '628 at the human M_2 mAChR

Modulator concentration	$[^{35}S]GTP\gamma S$ binding	ERK1/2 phosphorylation
NMS alone	9.47 ± 0.16	10.24 ± 0.16
+0.3 μM '628	9.51 ± 0.14	10.43 ± 0.15
+1 μM '628	9.69 ± 0.14	10.51 ± 0.15
+3 μM '628	10.01 ± 0.19	10.76 ± 0.18
+10 μM '628	10.22 ± 0.16	10.81 ± 0.29

pA_2 values: Negative logarithm of the antagonist potency value for inhibiting 50% of the response to an EC_{80} concentration of IXO.

Met77^{2,58} and Met406^{6,54}, are located on the extracellular side of the receptor on TM2 and TM6 (Fig. 6F). The change in the environment of the Met406^{6,54} is likely due to its interaction with the side chain of Trp422^{7,35}, which is predicted to stack with the triazolo-quinazolinone moiety of '628 (Fig. 6G). Furthermore, the cointegration of NMS with '628 induces a strong and well-defined Met77^{2,58} peak compared with the antagonist alone (Fig. 6E). The shift of Met77^{2,58} may reflect changes of the environment of Tyr80^{2,61} and Tyr83^{2,64} that are located on the same face of TM2 as the methionine and, in the docking pose, are predicted to interact with '628 (SI Appendix, Fig. S6). Importantly, Met77^{2,58} is located at the interface of TM2/TM3/TM7, and mutagenesis of the tyrosine residues suggests that this network is key to the cooperativity between allosteric and orthosteric compounds (18). Compound '628 additionally stabilizes changes in two methionine residues toward the intracellular part of the receptor, Met112^{3,41} and Met202^{5,54} (Fig. 6F). Here, '628 appears to enhance the capacity of NMS to stabilize the conformational changes of the TM3 hinge (45). This is supported by the appearance of a single Met112^{3,41} peak, indicating a more uniform conformation of TM3, compared with NMS bound alone (Fig. 6E). Although '628 displays little influence on Met202^{5,54} when coadministered with the potent inverse agonist tiotropium (Fig. 6B), the PAM significantly shifts the Met202^{5,54} NMS peak (Fig. 6E), coincidentally toward the position of tiotropium-bound state. It is possible that these spectral changes reflect the capacity of '628 to enhance NMS-mediated stabilization of the inactive conformation of the receptor (Fig. 6H). Together, these data suggest that the spectral modification of the methionines by '628 reflects changes in the structure and the dynamics of the allosteric network as well as the G-protein-coupling domain, which might account for the affinity and efficacy modulation '628 has on NMS.

Subtype Selectivity of '628 for the M_2 mAChR. A motivation of this study was the discovery of selective allosteric modulators of the M_2 subtype of the mAChR; thus, we investigated the selectivity profile of '628 across all five mAChRs. In [³H]NMS equilibrium binding assays, '628 retained its strong PAM effect against the M_2 subtype, with slight PAM ($M_{1,4}$ mAChR) or even a slight NAM effect ($M_{3,5}$ mAChRs) for high concentrations of '628 at the other subtypes (Fig. 7 and SI Appendix, Table S5). This observation of differential allostery between the PAM and the antagonist at the various mAChRs is further supported by kinetic studies. In saturation binding studies, no significant effect of 10 μM '628 was observed on [³H]NMS at the non- M_2 mAChRs (Table 2 and SI Appendix, Fig. S7 A–D). Furthermore, the dissociation rate of [³H]NMS from the different mAChR subtypes was measured. Unlike the M_2 subtype, where '628 reduced the K_{off} by 50-fold, a high concentration of '628 had no substantial effect on [³H]NMS dissociation, determined using isotopic dilution with atropine, at any of the non- M_2 mAChRs (Table 2 and SI Appendix, Fig. S7 E–H). A possible exception may be the M_4 mAChR, where radioligand dissociation was detectably slowed—although even here, the effect was only fourfold—much less than with the M_2 subtype (Table 2 and Fig. 3A vs. SI Appendix, Fig. S7G). Perhaps this is not surprising, since the M_4 mAChR shows the highest sequence homology with the M_2 mAChR. Our results suggest that '628 is a selective modu-

lator for NMS at the M_2 mAChR, and either inactive or weakly active at the remaining mAChR subtypes.

PAM Effect of '628 on Native Tissue Membranes. To determine the utility of '628 as a probe in physiological systems, we examined the effect of '628 on an endogenous ligand (ACh) and a commonly used potent agonist (IXO) in functional assays. The effect of high concentrations (3 and 10 μM) of '628 was tested on both ACh-mediated (Fig. 4B and SI Appendix, Fig. S3 C, E, G, and I) or IXO-mediated (SI Appendix, Fig. S3 B, D, F, H, and J) ERK1/2 phosphorylation at M_{1-5} mAChRs, and no significant effects were observed at any of the receptors. These findings suggest either a lack of interaction of '628, or a NAL effect on endogenous signaling at all of the mAChR subtypes, making '628 an excellent tool compound to probe antagonist action in physiological systems.

To investigate the potential physiological relevance of the PAM effects of '628 on M_2 mAChR antagonists, we determined the effects of the modulator in the absence or presence of NMS on agonist-mediated [³⁵S]GTP γ S binding using membranes derived from rat hypothalamus and neonatal rat ventricular cardiomyocytes, which both natively express high levels of M_2 mAChRs (46, 47). We investigated the potentiation of NMS antagonism by '628 using both the potent agonist IXO in rat hypothalamic membranes (Fig. 8A), and on '628's potentiation of the same antagonist against the endogenous neurotransmitter, ACh, in neonatal rat ventricular cardiomyocytes (Fig. 8B). In the hypothalamic membranes with IXO, '628 potentiated NMS potency with a cooperativity of $\text{Log}\alpha_{NMS} = 1.10 \pm 0.31$, while in cardiomyocytes the cooperativity was $\text{Log}\alpha_{NMS} = 0.56 \pm 0.42$.

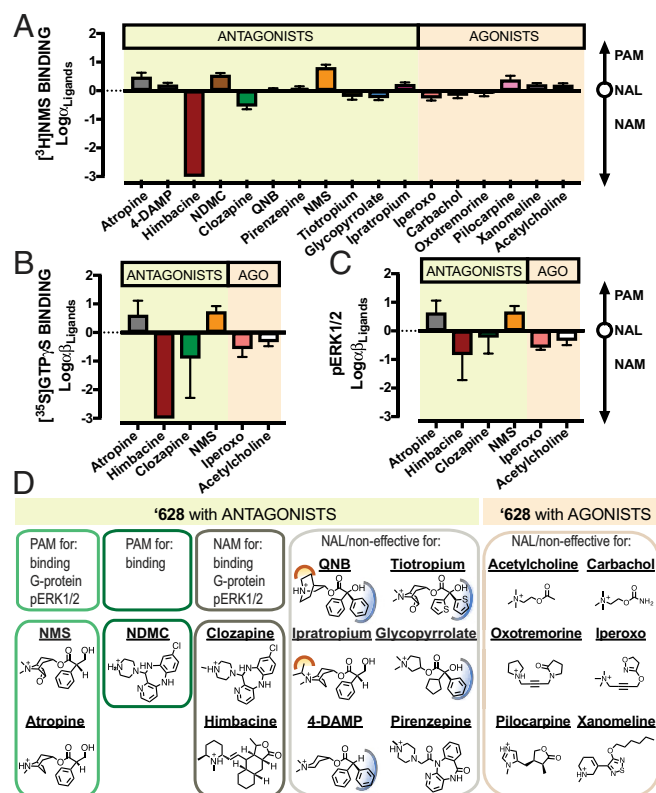


Fig. 5. Probe dependence of '628 with a panel of antagonists and agonists. (A) Cooperativity estimates of '628 with each indicated ligand determined using [³H]NMS equilibrium binding assays (complete dataset shown in SI Appendix, Fig. S4). Functional cooperativity estimates of '628 with selected antagonists determined in (B) [³⁵S]GTP γ S binding assays or (C) ERK1/2 phosphorylation assays. Full dataset shown in SI Appendix, Fig. S5. (D) Chemical structures of all ligands investigated and their classification in terms of the allosteric effect induced by '628 at the M_2 mAChR.

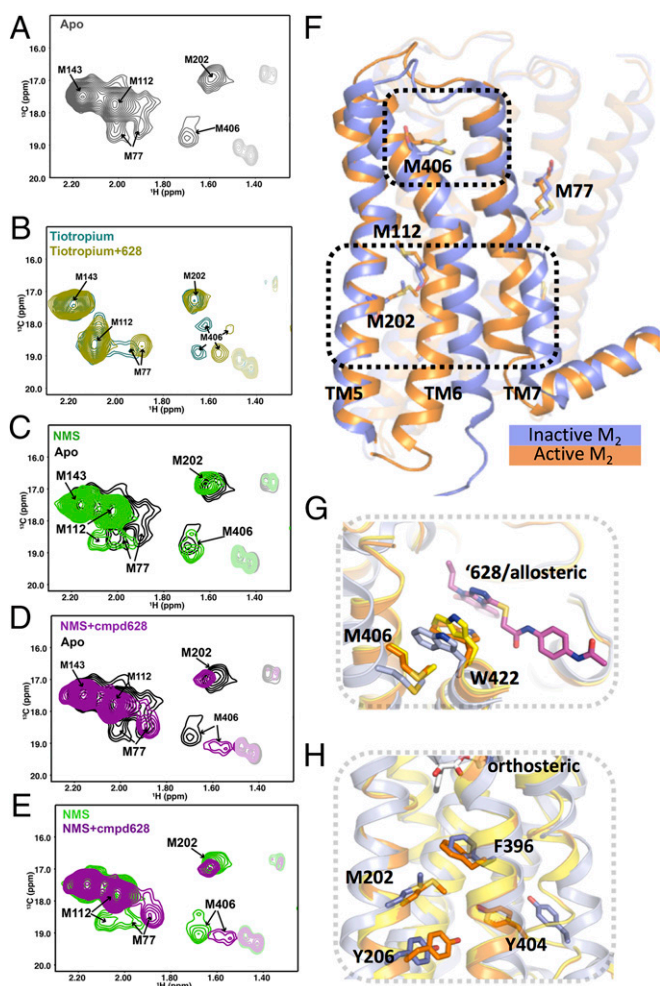


Fig. 6. The coincubation of '628 with NMS resulted in spectral shift of four methionine residues of the M_2 mAChR: Met77^{2,58}, Met112^{3,41}, Met202^{5,54}, and Met406^{6,54}. (A) Chemical shifts for five methionines of the Apo M_2 mAChR are shown (Met77^{2,58}, Met112^{3,41}, Met143^{4,44}, Met202^{5,54}, and Met406^{6,54}). (B) The superposition of the different spectral shifts for tiotropium (cyan) or tiotropium incubated with '628 (green). Different spectral shifts of the Apo spectra (black) with (C) NMS alone (green), (D) with NMS coincubated with allosteric compound '628 (purple), or (E) the latter two together. (F) The M_2 mAChR indicating the location of the four methionines augmented by '628 when coincubated with NMS [active (blue), inactive (orange) structure and agonist/PAM (yellow); PDB ID codes 4mq5, 4mq4, and 3uon, respectively] with close-up for (G) Met406^{6,54} and (D) Met202^{5,54} provided.

Encouragingly, and despite species effects that are common for allosteric ligands, no substantial difference was observed in the cooperativity between human and rat M_2 mAChRs across both binding and functional assays (Fig. 8C).

Discussion

Two key observations emerge from this study. First, allosteric sites in GPCRs can be targeted by structure-based, large library screens. This was far from certain to us at the outset of this project. Unlike orthosteric sites, whose relatively constrained structures have proven amenable to docking screens (48–56), the mAChR allosteric sites are less defined sterically, are open to bulk solvent, and are more conformationally labile in response to orthosteric ligand binding than are the orthosteric sites themselves. Nonetheless, 3 of 13 docking-prioritized molecules from the initial screen acted as modulators of antagonist (hit rate of 23%). While the potencies and PAM efficacies of the initial docked compounds were modest, the optimized PAM has an EC_{50} value and an α -factor that are not

far removed from widely used reagents like BPOA and LY2033298, and even medicines like cinacalcet (57, 58). Second, antagonist PAMs can confer specificity on orthosteric drugs that would otherwise lack it (7). Thus, by itself, scopolamine binds with similar affinity to all five receptor subtypes (K_D : 0.4–2.1 nmol/L) (24). Exploiting the specificity potential of the allosteric site, a PAM like '628, which on its own has no detectable signaling effect nor, crucially, does it modulate agonists, preferentially enhances antagonist binding at M_2 mACh over the other receptor subtypes. This suggests a general strategy to confer specificity onto potent but nonselective GPCR orthosteric drugs.

Although the sequence variability in the extracellular allosteric sites of the mAChRs makes them good targets for selective targeting in principle, the sites nonetheless present druggability challenges. In the inactive state, the allosteric sites are more open to solvent and less sterically defined than the orthosteric sites, as supported by the fact that prior, empirically discovered, inactive-state modulators, such as gallamine, alcuronium, and W-84 (41, 59), are often large and occasionally floppy. Even here, these challenges are reflected in the relatively high molecular weights of the antagonist PAMs that emerged, and their still modest affinities. We suspect that this will be often true for GPCR allosteric sites—both in the extracellular vestibule that we have targeted here (17), and in the sites emerging from new crystal structures (60–66). While GPCR allostery presents genuine opportunities for conferring selectivity and for compounds that lack the tonic liabilities of orthosteric-active molecules, allosteric sites may often be more challenging for identifying ligands with good physical properties when pursuing antagonist PAMs. Nonetheless, the ability to discover effective modulators for antagonists, and to optimize them without new synthesis, suggests that these sites remain accessible to structure-based discovery.

An important feature of these allosteric modulators is their chemical novelty—they do not resemble any known mAChR ligand chemotype for any subtype of which we are aware. Neither the original lead '589, nor the optimized analog, '628, display more than 0.28 EFCP4 Tanimoto coefficient (Tc) similarity to any mAChR ligand in ChEMBL (6,780 compounds both active and inactive), supporting the novelty of the triazolo-quinazolinones. This reflects the value of large library screens, especially compared with smaller chemical library screens targeting the same well-studied family. For example, a recent virtual screen of the ~1,600 compound National Cancer Institute diversity library against the M_2 mAChR found two novel allosteric ligands, NSC-322661 and NSC-13316 (20), but these molecules are also active against nine other GPCRs (i.e., NPY-Y1, NPY-Y2, GPR7, OXTR, MOR, DOR, 5HT5A, D1DR, S1P4, and even the M_1 mAChR). Conversely, not only are '589 and '628 dissimilar to other mAChR ligands, they have not been characterized as ligands for any other target in ZINC or ChEMBL. The antagonist PAM '628 thus has promise as a specific tool compound for the M_2 mAChR, transferring its selectivity in a probe-specific manner to the M_2 mAChR antagonists that it potentiates: NMS, atropine, and NDMC.

Certain caveats bear mentioning. First, our SAR studies around the triazolo-quinazolinone series were limited to molecules already

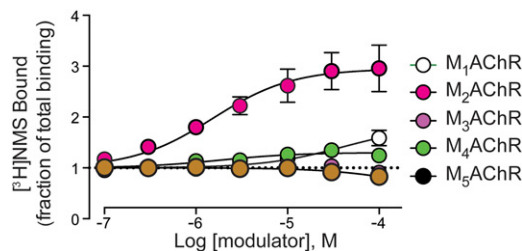


Fig. 7. Subtype selectivity of PAM '628 for [³H]NMS at the M_2 mAChR over M_1 , M_2 , M_4 , and M_5 . Increasing concentrations of modulator '628 were incubated at room temperature for 16 h with membranes from CHO cells expressing M_1 – M_5 mAChR subtypes at a single concentration of [³H]NMS at the K_D concentration for the receptor subtype. Specific binding was measured, and curves were fit using GraphPad Prism to determine the EC_{50} and maximal stimulation values for '628.

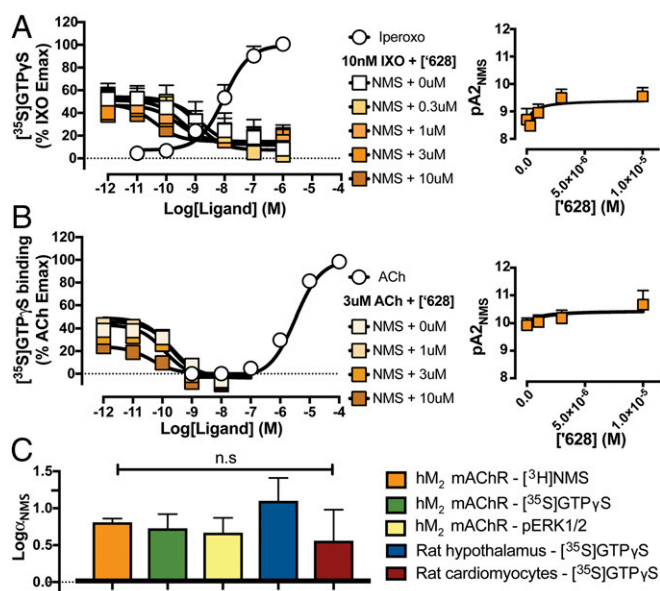


Fig. 8. Ex vivo validation of '628 as a PAM of NMS in native rat tissues expressing the M₂ mAChR. [³⁵S]GTPγS binding was determined (A) in rat hypothalamus membranes, where '628 was able to increase the affinity of NMS when tested against an EC₅₀ concentration of IXO, or (B) where similar experiments were performed in rat neonatal cardiomyocytes membranes, ACh as the agonist. (C) Statistical comparison of the cooperativity estimates of '628 as a PAM of NMS determined in five different experimental paradigms, using both human and native rat M₂ mAChRs.

available from vendors—we do not claim to have fully explored the SAR of this series, nor that '628 represents a fully optimized probe or lead. Thus, while the affinity and cooperativity of this molecule are within range of optimized PAMs from other series, on mAChRs and on other receptors, its physical properties may not be optimal for use as an in vivo probe. Also, it would be important to counter-screen the molecule for off-target effects from outside the muscarinic GPCR family. This can be done by testing activity against GPCR (67) and kinase (68) panels, as well as against side-effect target panels (69). Even wider nets for off-targets may be cast computationally (70)—all of these screens can help reduce the likelihood that a biological effect of a compound like '628 is mediated by an unexpected target, which would reduce its reliability as a probe. Other than testing against muscarinic receptor subtypes, none of these off-target tests have been conducted here. A second caveat is that when a molecule like '628 is used to confer specificity on a second, orthosteric antagonist like NMS that ordinarily would be nonspecific, concerns of differential metabolism of the two molecules can arise—this is most pressing for in vivo uses of the combination. Finally, whereas the methionine NMR supports the binding of '628 in the extracellular vestibular allosteric site of the M₂ mAChR, the atomic resolution accuracy of the docking models remains to be fully tested.

These caveats should not obscure the main observations of this study. Despite sites that are admittedly more challenging than many GPCR orthosteric sites, the extracellular vestibules of mAChRs remain accessible to structure-based discovery. In large library docking screens it is possible to find unprecedented scaffolds for these sites that can be optimized to a level of subtype selectivity inaccessible to most orthosteric antagonists. Through cooperativity with such (classically nonselective) orthosteric antagonists, these PAMs can confer selectivity on otherwise potent and highly efficacious drugs. Importantly, the optimized modulator, '628, consistently acted as an antagonist PAM while an agonist NAL at human and rodent M₂ mAChRs, in native tissues, and across multiple assays. Thus, the effect is robust to assay and to species variation, which has not always been true for allosteric modulators. This suggests a general strategy for conferring selectivity to orthosteric drugs of the family A GPCRs, especially those

older therapeutics that often suffer from intrafamily off-target effects but are otherwise potent and efficacious therapeutics.

Materials and Methods

See the *SI Appendix* for data analysis.

Molecular Docking Screen. We used the inactive state structure of M₂ mAChR in complex with QNB (PDB ID code 3UON). The receptor was prepared for docking by keeping just the M₂ residues (residues 20–48, 56–124, 135–210, and 384–444), while removing residues in the intracellular section that encompass the T4 lysozyme used to facilitate crystallization. All water molecules, ions, and the orthostatic ligand were removed. To indicate the position of the allosteric binding site, an input xtal-ligand was created by (i) placing two phenyl rings in perfect π -stacking distance (parallel face-centered and perpendicular y-shaped) from Tyr177^{ECL2}, (ii) placing a naphthalene structure parallel to Trp422^{7.35} and a phenyl ring in perpendicular t-shaped stacking conformation, and (iii) placing one phenyl ring in π - σ interaction with Thr187^{5.40} and π -alkyl interaction with Val408^{6.57} and Ala184^{5.37}. These atoms were used as the input into the SPHGEN program (71) to calculate a 60 spheres set that represent the allosteric site. This matching sphere set was later used to superimpose compounds from the virtual screening library and generate ligand poses. Following this, the automatic target preparation script were run to prepare the receptor (72). More specifically, the receptor polar atoms were protonated using REDUCE (73); however, the side chains were restricted to the original rotamer orientations with flipping turned off. To calculate the grid maps for scoring, three programs were used: CHEMGRID (34) was used to generate the van der Waals complementarity maps using the united-atom AMBER force-field (74); QNIFFT (35) was used, which implements the Poisson–Boltzmann equation to generate electrostatics grids; and SOLVMAP (32) was used to generate the ligand desolvation grid. Over 4.6 million commercially available lead-like molecules ($xlogP \leq 3.5$; molecular weight, ≤ 350 amu; and ≤ 7 rotatable bonds) (28) were docked using DOCK3.6 (32, 33, 75). Each compound was sourced from the ZINC database (76), which stores precalculated conformations and grids for flexible ligand docking. Ligands were matched in all orientations within the allosteric site that allow for four-point superposition of the rigid fragment onto the matching sphere set. For each compound, only a single top scoring pose was retained based on the scoring function that is composed of electrostatic interaction energies, van der Waals complementarity, and corrected for ligand desolvation. The parameters used for docking were as follows: receptor and ligand bin sizes of 0.4 Å, an overlap of 0.1–0.2 Å, a bump allowance of 1, a distance tolerance of 1.5 Å, labeled matching turned on, and 250 cycles of rigid-body minimization. From the top 2,500 scoring molecules, any compounds extending beyond the allosteric vestibule was omitted (Fig. 1A, cyan surface). Next, all other compounds were visually inspected; molecules with unsatisfied polar interactions, or with low hit diversity, were rejected. Finally, 38 compounds were chosen for the hit picking party, from which 13 compounds were purchased for testing.

For docking of the analog-by-catalog compounds, DOCK3.7 (37) was used with both the inactive (PDB ID code 3UON) and active structures (PDB ID code 4MQT) of M₂ mAChR. The M₂ mAChR inactive structure was prepared for docking as previously described; however, the matching sphere set was used as the xtal-ligand input. The active M₂ mAChR structure complexed with IXO and LY2119620 was prepared using residues 20–214 and 379–456 for target. Furthermore, the orthosteric ligand (agonist), IXO, was retained as a coligand during docking and was prepared using PRODRG server (77), while the allosteric compound was used as the xtal-ligand. Based on the docking poses of the available analogs in the ZINC database, 16 compounds were chosen for further investigation (*Discussion*, Table 1, and *SI Appendix*, Table S2).

The two NAM compounds were purchased from Specs (catalog no. AE-848/42025900) ('029) and from Vitas-M (catalog no. STK816972), while the PAM '589 was acquired from Enamine (catalog no. Z324823878). The purity of the most efficacious PAMs, '563 (Enamine; catalog no. Z16439559) and '628 (Enamine; catalog no. 16439767), was determined by mass spectroscopy (*SI Appendix*, Fig. S2), indicating that both compounds were >98% homogeneous by weight.

Colloidal Aggregation. Molecules were tested for colloidal aggregation by measuring scattering by dynamic light scattering (DLS) and by measuring nonspecific enzyme inhibition in an AmpC β -lactamase counterscreen (38, 39, 78, 79). Concentrations from 25 to 100 μ M were tested for '589 and '628. At concentration above 25 μ M '628 in 10 mM Hepes, pH 7.5, and 1% DMSO, the solutions had to be heated to 42 °C for '628 to dissolve the compound. Additives, such as PEG-300 and solutol, can be used to solubilize the compound above 100 μ M. AmpC β -lactamase counterscreen with '589 and '628 concentrations of up to 100 μ M retained enzyme activity of above 90%.

NMR Methods. The human M₂ mAChR construct M2RΔ5M was expressed, labeled, and purified. Briefly, the receptor was expressed in Sf9 cells using Bac-to-Bac baculovirus system. Cells were grown in methionine-deficient medium (Expression System) and infected at a density of 4×10^6 mL⁻¹. ¹³CH₃E-methionine was added into the medium during infection for specific labeling. The M₂ mAChR receptor was purified by Ni-NTA chromatography, Flag affinity chromatography, and size exclusion chromatography sequentially. The final NMR sample was prepared in a buffer prepared in D₂O containing 20 mM Hepes, 100 mM NaCl, 0.01% (wt/vol) lauryl maltose neopentyl glycol (Anatrace), and 0.003% (wt/vol) cholesterol hemisuccinate (Sigma), and was concentrated to around 100 μM at a volume of ~250 μL. The NMR data collection and assignment of methionine methyl ¹H-¹³C resonances of M₂ mAChRΔ5M were conducted. All NMR experiments were performed at 25 °C on a Bruker Avance 800-MHz spectrometer equipped with a cryogenic probe.

The spectra of M₂ mAChR bound to different antagonist and '628 were acquired by the following procedure. All ligands were dissolved in perdeuterated dimethyl d6-sulfoxide (DMSO-d₆). NMS or tiotropium was added to the receptor at a saturation concentration of 1 mM. The ¹H-¹³C heteronuclear single-quantum coherence (HSQC) spectra of M₂ mAChRs bound to either antagonist were collected. After the NMR experiments in scopolamine- or tiotropium-bound states, '628 was added to the antagonist-bound sample at a final concentration of 250 μM, and the ¹H-¹³C HSQC spectra were further collected. The total collection time for each single experiment was around 10 h. All NMR spectra were processed using the software package NMRPipe (80) and visualized using the program NMRViewJ.

Radioligand Binding Assays. In our original biological screen to validate our VLS method, cell membranes from CHO cells expressing M₂ mAChR were incubated for 1.5 h at 25 °C with 0.2 nM [³H]NMS, in absence or presence of either a fixed concentration of our VLS selected hits, LY2119620 or gallamine at 10 μM, in binding assay buffer containing 10 mM Hepes, pH 7.4, 10 mM NaCl, and 0.5 mM MgCl₂. Further characterization of '589 and its analog-by-catalog series was performed under identical conditions, but with increasing concentrations of each putative modulator, ranging from 0 to 100 μM. For the probe dependence study, radioligand binding was performed with identical concentration of [³H]NMS as described above, but on intact CHO cells expressing the M₂ mAChR, and incubated for 6 h at 21 °C.

For saturation binding assays, cell membranes from CHO cells expressing either M₁–M₅ human AChR (for M₃, an M3RΔICL3 construct was used) were incubated for 2 h at 25 °C with 0–2.5 nM [³H]NMS or 0–0.25 nM [³H]IXO, and 0–100 μM test compound or 10 μM atropine (to determine nonspecific binding) in binding assay buffer. Samples were harvested on GF/C filter plates, quickly washed with cold assay buffer, and dried, and liquid scintillation mixture was added to determine radioactivity retained on the filters.

Radioligand Kinetic Dissociation Binding Assays. Cell membranes from CHO cells expressing either M₁–M₅ AChR (for M₃, an M3RΔICL3 construct was used) were incubated for 60 min at 25 °C with 0.2 nM [³H]NMS in binding buffer. Atropine (20 μM) with 0–100 μM test compound was added to determine dissociation for the indicated times. Samples were harvested, washed, and counted. Shown are combined results from three separate experiments.

- Santos R, et al. (2017) A comprehensive map of molecular drug targets. *Nat Rev Drug Discov* 16:19–34.
- Foster DJ, Conn PJ (2017) Allosteric modulation of GPCRs: New insights and potential utility for treatment of schizophrenia and other CNS disorders. *Neuron* 94:431–446.
- Bradley SJ, et al. (2017) M1 muscarinic allosteric modulators slow prion neurodegeneration and restore memory loss. *J Clin Invest* 127:487–499.
- Schmäl F (2013) Neuronal mechanisms and the treatment of motion sickness. *Pharmacology* 91:229–241.
- Price D, Fromer L, Kaplan A, van der Molen T, Román-Rodríguez M (2014) Is there a rationale and role for long-acting anticholinergic bronchodilators in asthma? *NPJ Prim Care Respir Med* 24:14023.
- Andersson KE (2004) Antimuscarinics for treatment of overactive bladder. *Lancet Neurol* 3:46–53.
- Caulfield MP, Birdsall NJ (1998) International Union of Pharmacology. XVII. Classification of muscarinic acetylcholine receptors. *Pharmacol Rev* 50:279–290.
- Naicker P, Anoopkumar-Dukie S, Grant GD, Kavanagh JJ (2017) Anticholinergic activity in the nervous system: Consequences for visuomotor function. *Physiol Behav* 170:6–11.
- Glavind K, Chancellor M (2011) Antimuscarinics for the treatment of overactive bladder: Understanding the role of muscarinic subtype selectivity. *Int Urogynecol J* 22:907–917.
- Grover AK (2013) Use of allosteric targets in the discovery of safer drugs. *Med Princ Pract* 22:418–426.
- Gentry PR, Sexton PM, Christopoulos A (2015) Novel allosteric modulators of G protein-coupled receptors. *J Biol Chem* 290:19478–19488.

[³⁵S]GTPγS Binding Assay. Membrane homogenates (15 μg) were equilibrated in a 500-μL total volume of assay buffer containing 10 μM GDP and a range of concentrations of agonists, in the absence or presence of increasing concentrations of allosteric modulator for simple agonist versus allosteric ligand interaction. To assess the effect of '628 on antagonist affinity, we used an EC₈₀ concentration of agonist (either ACh or IXO) in presence of increasing concentrations of antagonists (NMS, atropine, himbacine, or clozapine) in absence or presence of increasing concentrations of modulator. In all cases, the assays were incubated at 30 °C for a period of 1 h, prior addition of 50 μL of [³⁵S]GTPγS (0.3–1 nM) for a further 30 min.

[³⁵S]GTPγS Binding Assay Following Overnight Pretreatment. Cell membranes (12–18 μg) from CHO-M₂ cells were incubated overnight at room temperature with 0–100 μM acetylcholine or 0–1 μM IXO, and 10 μM '628 or DMSO vehicle in assay buffer containing 10 mM Hepes, pH 7.4, 100 mM NaCl, and 5 mM MgCl₂. Then, [³⁵S]GTPγS and GDP were added to get final concentrations of 0.1 nM [³⁵S]GTPγS and 30 μM GDP and then incubated for 1 h at 30 °C. Samples were harvested, washed, and counted. Figures show the combined results from three separate experiments, performed in duplicate.

Extracellular Signal-Regulated Kinase 1/2 Phosphorylation Assays. Initial ERK1/2 phosphorylation time course experiments were performed to determine the time at which ERK1/2 phosphorylation was maximal after stimulation by each ligand. Cells were seeded into transparent 96-well plates at 20,000 cells per well and grown for over 8 h. Cells were then washed once with PBS and incubated in serum-free DMEM at 37 °C overnight to allow FBS-stimulated phosphorylated ERK1/2 levels to subside. Cells were then stimulated for 25 min without or with antagonist, followed by a 5-min agonist incubation at 37 °C in 5% CO₂. For all experiments, 10% (vol/vol) FBS was used as a positive control, and vehicle controls were also performed. The reaction was terminated by removal of drugs and lysis of cells with 100 μL of SureFire lysis buffer (TGR Biosciences), and 5 μL of this lysate was added in a 384-well white ProxiPlate (PerkinElmer). A mixture of SureFire activation buffer, SureFire reaction buffer, and AlphaScreen beads was prepared in a ratio of 100:600:3 (vol/vol/vol) and added to the lysate for a lysate/mixture ratio of 5:8 (vol/vol). Plates were incubated for 1–1.5 h at 37 °C before the fluorescence signal was measured on a Fusion-α plate reader (PerkinElmer) using standard AlphaScreen settings.

ACKNOWLEDGMENTS. We thank Dr. Anat Levit for fruitful discussions and for comments about this manuscript. We also thank the NMR facility support at the Beijing NMR Center and the NMR facility of National Center for Protein Sciences at Peking University. This work was supported by Grant GM106990 (to B.K.K., R.K.S., and B.K.S.) and by Program Grant APP105134 of the National Health and Medical Research Council (NHMRC) of Australia (to A.C. and P.M.S.), NHMRC Project Grant APP1082318 (to C.V.), and Australian Research Council Future Fellowship FT140100114 (to C.V.). A.C. is a Senior Principal, and P.M.S., a Principal, Research Fellow of the NHMRC. C.V. is an Australian Research Council Future Fellow.

- Lüllmann H, Ohnesorge FK, Schauwecker GC, Wassermann O (1969) Inhibition of the actions of carbachol and DFP on guinea pig isolated atria by alkane-bis-ammonium compounds. *Eur J Pharmacol* 6:241–247.
- Valant C, Felder CC, Sexton PM, Christopoulos A (2012) Probe dependence in the allosteric modulation of a G protein-coupled receptor: Implications for detection and validation of allosteric ligand effects. *Mol Pharmacol* 81:41–52.
- Tränkle C, et al. (2003) Interactions of orthosteric and allosteric ligands with [³H]dimethyl-W84 at the common allosteric site of muscarinic M2 receptors. *Mol Pharmacol* 64:180–190.
- Lroy CH, et al. (2014) Characterization of the novel positive allosteric modulator, LY2119620, at the muscarinic M₂ and M₄ receptors. *Mol Pharmacol* 86:106–115.
- Clark AL, Mitchelson F (1976) The inhibitory effect of gallamine on muscarinic receptors. *Br J Pharmacol* 58:323–331.
- Kruse AC, et al. (2013) Activation and allosteric modulation of a muscarinic acetylcholine receptor. *Nature* 504:101–106.
- Thal DM, et al. (2016) Crystal structures of the M1 and M4 muscarinic acetylcholine receptors. *Nature* 531:335–340.
- Haga K, et al. (2012) Structure of the human M2 muscarinic acetylcholine receptor bound to an antagonist. *Nature* 482:547–551.
- Miao Y, et al. (2016) Accelerated structure-based design of chemically diverse allosteric modulators of a muscarinic G protein-coupled receptor. *Proc Natl Acad Sci USA* 113:E5675–E5684.
- Gentry PR, et al. (2014) Development of a highly potent, novel M5 positive allosteric modulator (PAM) demonstrating CNS exposure: 1-((1H-indazol-5-yl)sulfonyl)-N-ethyl-N-

- (2-(trifluoromethyl)benzyl)piperidine-4-carboxamide (ML380). *J Med Chem* 57: 7804–7810.
22. Davoren JE, et al. (2016) Discovery of the potent and selective M1 PAM-agonist *N*-[(3*R*,4*S*)-3-hydroxytetrahydro-2*H*-pyran-4-yl]-5-methyl-4-[4-(1,3-thiazol-4-yl)benzyl]pyridine-2-carboxamide (PF-06767832): Evaluation of efficacy and cholinergic side effects. *J Med Chem* 59:6313–6328.
23. Witkin JM, et al. (2014) M₁ and M₂ muscarinic receptor subtypes regulate antidepressant-like effects of the rapidly acting antidepressant scopolamine. *J Pharmacol Exp Ther* 351: 448–456.
24. Hasselmann H (2014) Scopolamine and depression: A role for muscarinic antagonism? *CNS Neurol Disord Drug Targets* 13:673–683.
25. Gerhard DM, Wohleb ES, Duman RS (2016) Emerging treatment mechanisms for depression: Focus on glutamate and synaptic plasticity. *Drug Discov Today* 21: 454–464.
26. Charlton M, Thompson JP (2016) Drugs affecting the autonomic nervous system. *Anaesthesia Intensive Care Med* 17:575–580.
27. Oprea TI, Davis AM, Teague SJ, Leeson PD (2001) Is there a difference between leads and drugs? A historical perspective. *J Chem Inf Comput Sci* 41:1308–1315.
28. Irwin JJ, Shoichet BK (2005) Hierarchical docking of commercially available compounds for virtual screening. *J Chem Inf Model* 45:177–182.
29. Sterling T, Irwin JJ (2015) ZINC 15—ligand discovery for everyone. *J Chem Inf Model* 55:2324–2337.
30. Li JB, et al. (1999) Extension of the platform of applicability of the SM5.42R universal solvation model. *Theor Chem Acc* 103:9–63.
31. Kruse AC, et al. (2012) Structure and dynamics of the M3 muscarinic acetylcholine receptor. *Nature* 482:552–556.
32. Mysinger MM, Shoichet BK (2010) Rapid context-dependent ligand desolvation in molecular docking. *J Chem Inf Model* 50:1561–1573.
33. Lorber DM, Shoichet BK (2005) Hierarchical docking of databases of multiple ligand conformations. *Curr Top Med Chem* 5:739–749.
34. Meng EC, Shoichet BK, Kuntz ID (1992) Automated docking with grid-based energy evaluation. *J Comput Chem* 13:505–524.
35. Gallagher K, Sharp K (1998) Electrostatic contributions to heat capacity changes of DNA-ligand binding. *Biophys J* 75:769–776.
36. Sharp KA (1995) Polyelectrolyte electrostatics—salt dependence, entropic, and enthalpic contributions to free-energy in the nonlinear Poisson-Boltzmann model. *Biopolymers* 36:227–243.
37. Coleman RG, Carchia M, Sterling T, Irwin JJ, Shoichet BK (2013) Ligand pose and orientational sampling in molecular docking. *PLoS One* 8:e75992.
38. Irwin JJ, et al. (2015) An aggregation advisor for ligand discovery. *J Med Chem* 58: 7076–7087.
39. McGovern SL, Caselli E, Grigorieff N, Shoichet BK (2002) A common mechanism underlying promiscuous inhibitors from virtual and high-throughput screening. *J Med Chem* 45:1712–1722.
40. Gnagay AL, Seidenberg M, Ellis J (1999) Site-directed mutagenesis reveals two epitopes involved in the subtype selectivity of the allosteric interactions of gallamine at muscarinic acetylcholine receptors. *Mol Pharmacol* 56:1245–1253.
41. Dror RO, et al. (2013) Structural basis for modulation of a G-protein-coupled receptor by allosteric drugs. *Nature* 503:295–299.
42. Lane JR, May LT, Parton RG, Sexton PM, Christopoulos A (2017) A kinetic view of GPCR allostery and biased agonism. *Nat Chem Biol* 13:929–937.
43. Christopoulos A (2014) Advances in G protein-coupled receptor allostery: From function to structure. *Mol Pharmacol* 86:463–478.
44. Lee NH, el-Fakahany EE (1990) The allosteric binding profile of himbacine: A comparison with other cardioselective muscarinic antagonists. *Eur J Pharmacol* 179: 225–229.
45. Lans I, Dalton JAR, Giraldo J (2015) Helix 3 acts as a conformational hinge in class A GPCR activation: An analysis of interhelical interaction energies in crystal structures. *J Struct Biol* 192:545–553.
46. Colecraft HM, Egamino JP, Sharma VK, Sheu SS (1998) Signaling mechanisms underlying muscarinic receptor-mediated increase in contraction rate in cultured heart cells. *J Biol Chem* 273:32158–32166.
47. Jagoda EM, et al. (2003) Regional brain uptake of the muscarinic ligand, [¹⁸F]FP-TZTP, is greatly decreased in M2 receptor knockout mice but not in M1, M3 and M4 receptor knockout mice. *Neuropharmacology* 44:653–661.
48. Kolb P, et al. (2009) Structure-based discovery of β_2 -adrenergic receptor ligands. *Proc Natl Acad Sci USA* 106:6843–6848.
49. Carlsson J, et al. (2010) Structure-based discovery of A2A adenosine receptor ligands. *J Med Chem* 53:3748–3755.
50. Weiss DR, et al. (2013) Conformation guides molecular efficacy in docking screens of activated β_2 adrenergic G protein coupled receptor. *ACS Chem Biol* 8:1018–1026.
51. Manglik A, et al. (2016) Structure-based discovery of opioid analgesics with reduced side effects. *Nature* 537:185–190.
52. Katritch V, et al. (2010) Structure-based discovery of novel chemotypes for adenosine A_{2A} receptor antagonists. *J Med Chem* 53:1799–1809.
53. Kooistra AJ, et al. (2016) Function-specific virtual screening for GPCR ligands using a combined scoring method. *Sci Rep* 6:28288.
54. Negri A, et al. (2013) Discovery of a novel selective kappa-opioid receptor agonist using crystal structure-based virtual screening. *J Chem Inf Model* 53:521–526.
55. Ranganathan A, et al. (2017) Ligand discovery for a peptide-binding GPCR by structure-based screening of fragment- and lead-like chemical libraries. *ACS Chem Biol* 12:735–745.
56. Langmead CJ, et al. (2012) Identification of novel adenosine A_{2A} receptor antagonists by virtual screening. *J Med Chem* 55:1904–1909.
57. Davey AE, et al. (2012) Positive and negative allosteric modulators promote biased signaling at the calcium-sensing receptor. *Endocrinology* 153:1232–1241.
58. Leach K, et al. (2016) Towards a structural understanding of allosteric drugs at the human calcium-sensing receptor. *Cell Res* 26:574–592.
59. Jakubik J, El-Fakahany EE (2010) Allosteric modulation of muscarinic acetylcholine receptors. *Pharmaceuticals (Basel)* 3:2838–2860.
60. Dore AS, et al. (2017) Decoding corticotropin-releasing factor receptor type 1 crystal structures. *Curr Mol Pharmacol* 10:334–344.
61. Oswald C, et al. (2016) Intracellular allosteric antagonism of the CCR9 receptor. *Nature* 540:462–465.
62. Zhang D, et al. (2015) Two disparate ligand-binding sites in the human P2Y1 receptor. *Nature* 520:317–321.
63. Jazayeri A, et al. (2016) Extra-helical binding site of a glucagon receptor antagonist. *Nature* 533:274–277.
64. Cheng RKY, et al. (2017) Structural insight into allosteric modulation of protease-activated receptor 2. *Nature* 545:112–115.
65. Zheng Y, et al. (2016) Structure of CC chemokine receptor 2 with orthosteric and allosteric antagonists. *Nature* 540:458–461.
66. Lu J, et al. (2017) Structural basis for the cooperative allosteric activation of the free fatty acid receptor GPR40. *Nat Struct Mol Biol* 24:570–577.
67. Huang XP, et al. (2015) Allosteric ligands for the pharmacologically dark receptors GPR68 and GPR65. *Nature* 527:477–483.
68. Lansu K, et al. (2017) In silico design of novel probes for the atypical opioid receptor MRGPRX2. *Nat Chem Biol* 13:529–536.
69. Bowes J, et al. (2012) Reducing safety-related drug attrition: The use of in vitro pharmacological profiling. *Nat Rev Drug Discov* 11:909–922.
70. Lounkine E, et al. (2012) Large-scale prediction and testing of drug activity on side-effect targets. *Nature* 486:361–367.
71. Kuntz ID, Blaney JM, Oatley SJ, Langridge R, Ferrin TE (1982) A geometric approach to macromolecule-ligand interactions. *J Mol Biol* 161:269–288.
72. Irwin JJ, et al. (2009) Automated docking screens: A feasibility study. *J Med Chem* 52: 5712–5720.
73. Word JM, Lovell SC, Richardson JS, Richardson DC (1999) Asparagine and glutamine: Using hydrogen atom contacts in the choice of side-chain amide orientation. *J Mol Biol* 285:1735–1747.
74. Pearlman DA, et al. (1995) Amber, a package of computer-programs for applying molecular mechanics, normal-mode analysis, molecular-dynamics and free-energy calculations to simulate the structural and energetic properties of molecules. *Comput Phys Commun* 91:1–41.
75. Wei BQ, Baase WA, Weaver LH, Matthews BW, Shoichet BK (2002) A model binding site for testing scoring functions in molecular docking. *J Mol Biol* 322:339–355.
76. Irwin JJ, Sterling T, Mysinger MM, Bolstad ES, Coleman RG (2012) ZINC: A free tool to discover chemistry for biology. *J Chem Inf Model* 52:1757–1768.
77. Schüttelkopf AW, van Aalten DM (2004) PRODRG: A tool for high-throughput crystallography of protein-ligand complexes. *Acta Crystallogr D Biol Crystallogr* 60:1355–1363.
78. Irwin JJ, Shoichet BK (2016) Docking screens for novel ligands conferring new biology. *J Med Chem* 59:4103–4120.
79. Duan D, Doak AK, Nedyalkova L, Shoichet BK (2015) Colloidal aggregation and the in vitro activity of traditional Chinese medicines. *ACS Chem Biol* 10:978–988.
80. Delaglio F, et al. (1995) NMRPipe: A multidimensional spectral processing system based on UNIX pipes. *J Biomol NMR* 6:277–293.